Original article

Institution of MECHANICAL ENGINEERS

Journal of PROCESS MECHANICAL ENGINEERING

Friction stir spot welding lap-shear force analysis of automotive low-carbon steel sheets joint

Proc IMechE Part E:
J Process Mechanical Engineering
1–11

DOI: 10.1177/09544089241234553
journals.sagepub.com/home/pie
Sage

Carlos E C Barbosa[1], Marcio Batista[1], Gilmar F Batalha[1], Rafael H M de Siqueira[1], Éd C Bordinassi[2], Adalto Farias[3] and Sergio Delijaicov[3]

Abstract

This study aims to provide reference values and outcomes to support the practical implementation of friction stir spot welding in the automotive industry. This study investigated the friction stir spot welding of AISI/SAE 1006 cold-rolled low-carbon steel sheets commonly used in automotive lightweight structural components. Employing a design of experiment-composite central design approach, process parameters like tool rotational speed, plunge depth, and dwell time were examined using a series of experiments. The friction stir spot welding process was conducted using a tungsten carbide M30 tool. The study analyzed the influence of these parameters on mechanical properties such as lap-shear force, axial force, torque, and temperature. Plunge depth showed as a statistically significant factor affecting axial force. Torque demonstrated sensitivity to plunge depth and tool rotational speed, while temperature primarily depended on tool rotational speed. The tool rotational speed and plunge depth combination led to substantial temperature increments, promoting thermal structural transformations, including recrystallization. The analyses of microstructures revealed distinct zones within the welded joint, highlighting the recrystallization phenomena primarily in the mixing zone beneath the tool. The results showed satisfactory mechanical joint quality with ductile failure modes. No significant correlation was found between the lap-shear force and the dependent parameters. The selected range of variables and the chosen tool profile suggest a viable approach for producing friction stir spot welding joints in low-carbon steel and a robustness of the process in achieving an average tensile lap-shear force of 7.48 ± 0.64 kN, surpassing the minimum specification stipulated in the American National Standard AWS D8.1 M, which is 1.5 kN. This finding highlights the complex nature of the friction stir spot welding process, suggesting that other factors beyond the investigated parameters may influence the lap-shear force and indicate the potential to achieve even higher tensile stress values in lap joints by exploring alternative parameter combinations.

Keywords

Friction stir spot welding, friction stir welding, automotive weld, friction stir spot welding, friction stir welding

Date received: 21 September 2023; accepted: 22 January 2024

Introduction

The regulatory landscape within the automotive industry, emphasizing emissions reduction, enhanced fuel efficiency,[3] and safety, has catalyzed a demand for sophisticated manufacturing methodologies capable of meeting the rigorous quality and cost criteria.[4,5] To meet the stringent demands for durability and sustainability in today's automobile industry, the development of new welding technologies, such as friction stir spot welding (FSSW), becomes imperative. FSSW is considered a specialized form of friction stir welding (FSW) process, characterized by the absence of lateral movement along the workpiece. This technique can produce high-quality, solid-state lap welds, specifically in sheet materials.[6,7]

Çapar et al.[6] summarised several advantages of FSSW in the automotive industry compared to fusıon weldıng for dissimilar materials concerning issues in fusion welding related to solidification process and structure, including loss of alloying elements and presence of segregation and porosities, blow hole, crack formation in the weld joint. FSSW is a promising alternative to traditional

[1]Mechanical Engineering Department, University of São Paulo – Escola Politécnica, São Paulo, SP, Brazil
[2]Mechanical Engineering Department, Instituto Mauá de Tecnologia, São Caetano do Sul, SP, Brazil
[3]Mechanical Engineering Department, Centro Universitário FEI, São Bernardo do Campo, SP, Brazil

Corresponding author:
Sergio Delijaicov, Centro Universitário FEI, Mechanical Engineering Departament, São Bernardo do Campo, SP, Brazil.
Email: sergiode@fei.edu.br

single-point joining methods such as resistance spot welding (RSW), widely used in the automotive industry, and self-riveting techniques. Its versatility in joining various materials, including steels, high-strength steel variants, and dissimilar materials like aluminium/steel,[3] effectively addresses the limitations of conventional methods. FSSW surpasses issues such as brittle microstructure formation caused by high welding temperatures and rapid cooling rates in RSW. According to Kumar et al. RSW has limitations regarding the electrode wearing out on multiple usages for joining of steels, and to overcome this, many new tools are coming up to join the steel material.[8]

Thin steel plates commonly utilized in the automotive industry, especially those with galvanized coatings, bring challenges for being joined by RSW due to the inadequate heat conduction caused by the galvanized coating and are suitable for FSSW applications. Andrade et al.[9] investigated the impact of varying galvanized coating thickness on the thermal cycles in thin steel plates commonly utilized in steel construction and the automotive industry by applying FSSW.

FSSW was first developed by Mazda Motor Corporation in 1993. It involves three stages[10]: Plunge, stirring, and retraction. The process starts with the tool rotating at a high tool rotational speed and being axially forced into the joint parts until the tool's shoulder contacts the upper surface, creating a spot weld. The plunging motion of the tool leads to the expulsion of excess materials. Subsequently, the agitation stage begins when the tool reaches the desired plunge depth. During this phase, the rotational movement of the tool generates frictional heat. Combined with the immersion stages, it heats, softens, and blends the materials adjacent to the tool, forming a solid-state joint. Once the desired bond is achieved, the tool retracts from the joint, leaving behind a keyhole. The presence of the keyhole represents a limitation in the FSSW process[10] due to the potential corrosion caused by liquid accumulation. To address this issue, Wang, Morisada, and Fujii,[11] as well as Wang et al.,[12] utilized double-side adjustable tools on 2 mm low carbon steel plates to create flat joints, thereby eliminating the formation of a keyhole observed in conventional FSSW.

According to Kumar et al.,[8] three essential parameters in the FSSW process are tool rotational speed, dwell time, and plunge depth. In their study involving dissimilar materials, aluminium alloy AA6062 with structural steel 1020 was welded to create lap joints for subsequent tensile test evaluations, yielding joints with tensile strength values of up to 5.65 kN. Their primary observation was that dwell time exhibits greater significance as a parameter compared to tool speed and plunge depth.

Feizollahi and Moghadam[3] evaluated three conical pins with varying lengths, along with different dwell times and rotation speeds of the tool. Their objective was to compare the simultaneous effects of several important process parameters on mechanical and welding properties. The tool penetration depth (pin length) was the most important parameter, followed by the rotation speed and dwell time.

Lakshminarayanan et al.[13] conducted a study on the optimal parameters for FSSW of 0.8 mm-thick low-carbon steel sheets using a flat cylindrical tool shoulder (with a diameter of 8 mm) and a tapered pin ranging from 3.2 to 1.6 mm. They emphasized the significant influence of dwell time on the joint properties, particularly the lap-shear force. Their findings indicated that the maximum lap-shear force of 15.67 kN was achieved at a tool rotational speed of 1157 r/min, a plunge depth of 0.005 mm, and a dwell time of 22 s.

In another study, Sun et al.[14] investigated the LT-FSSW (Low-Temperature FSSW) of 2 mm thick steel plate cold-rolled commercial (SPCC) low carbon steel plates under high applied load and shallow tool rotational speeds ranging from 5 to 50 r/min. Through lap-shear force tests, they observed that the joints reached a fracture load of 10 kN at a tool rotational speed of 20 r/min and a dwell time of 30 s.

Baek et al.[15] examined FSSW joints in low carbon steel plates with a lap configuration (0.6 mm-thick, 30 mm-wide, 100 mm-long) using a WC-Co alloy tool at a tool rotational speed of 1600 r/min and a tool plunge depth ranging from 0.12 to 0.30 mm. They concluded that the tool plunge depth significantly influenced the failure mode of the joined samples but had a weak effect on the joint shear strength. However, they obtained a relatively low average tensile lap-shear force value of 3.4 kN, which still exceeded the minimum requirement specified by the American National Standard AWS D8.1 M (1).

Feng et al.[16] investigated the feasibility of FSSW on advanced high-strength steel sheet metals with a thickness of 1.6 mm, utilizing a single tool consisting of a 2.0 mm long tapered pin and a 10 mm diameter shoulder made of polycrystalline cubic boron nitride. Their study highlighted the need for modifications in tool geometry to enhance joint strength.

In a study by Mazzaferro et al.,[17] FSSW butt joints were examined in 1.0 mm thick sheets of cold-rolled and electro-galvanized TRIP 800 steel. They employed a polycrystalline cubic boron nitride tool featuring a 15 mm diameter cylindrical concave shoulder and a conic pin with a diameter of 5 mm and a length of 1.5 mm. They concluded that the axial force and torque depended on the mechanical interactions between the tool and workpiece and could indicate process stability and weld quality. The highest lap-shear force was achieved by employing the lowest tool rotational speed and the highest dwell time in their welding condition.

This study analyzed the mechanical strength of FSSW joints with 1.4 mm total thickness AISI/SAE 1006 cold rolled steel. The aim was to evaluate the influence of tool rotational speed, plunge depth, and dwell time on the maximum tensile lap-shear force. A design of experiments (DOE) approach was employed to facilitate further analysis and discussions, specifically the composite central design (CCD) response surface methodology.

Table 1. Design of experiment (DOE) composite central design levels.

	α level	−1.682	−1	0	1	1.682
Tool rotational speed	(r/min)	1363	1500	1700	1900	2036
Plunge depth	(mm)	0.8	0.87	0.97	1.07	1.13
Dwell time	(s)	2.3	3.0	4.0	5.0	5.7

The process parameter ranges for investigation were as follows: tool rotational speed ranging from 1500 to 1900 r/min, dwell time ranging from 3 to 5 s, and plunge depth ranging from 0.87 to 1.07 mm. By systematically examining these parameters within the specified ranges, the study aimed to uncover the optimal combination that would yield the highest tensile lap-shear force. Through this comprehensive analysis, valuable insights were gained regarding the impact of these process variables on the joint strength and performance of FSSW in the given material.

Materials and methods

The material used in this study was AISI/SAE 1006 cold-rolled steel sheets with a thickness of 0.7 mm, which comply with the standards set by DIN EN 10139 (2). These sheets are classified as DC05 and are commonly employed in fabricating structural components for lightweight vehicles in the automotive manufacturing industry. The mechanical properties of the SAE 1006 base metal are yield strength (285 MPa), ultimate tensile strength (330 MPa), and elongation (20%).

The process parameters, particularly the tool rotational speed (r/min) and plunge depth (mm), were chosen based on the existing literature. Lakshminarayanan et al.[13] employed high tool rotational speeds of 1200–1600 r/min and plunge depths ranging from 0.04 to0.2 mm. They identified dwell time as a critical factor for increasing heat input during welding. Sun et al.[14] varied tool rotational speeds from 800 to 1200 r/min, while Baek et al.[15] utilized a rotational speed of 1600 r/min along with plunge depths ranging from 0.12 to 0.3 mm. However, considering the variability in plunge depth reported in the literature, it is essential to conduct dedicated tests specifically for plate thicknesses of 0.7 mm, considering the previous findings.

A DOE-CCD approach was employed with three replications at the central point to examine the influence of parameters on the mechanical properties of the joints. The corresponding levels of the parameters used can be found in Table 1.

The influence of plunge speed on friction stir spot welding (FSSW) is widely acknowledged as a significant factor. Increasing the plunge speed results in a greater temperature gradient at the weld joint and applies a higher axial force on the tool.[18] While higher plunge speeds offer enhanced productivity, they can reduce tool life and exacerbate the hook phenomenon, ultimately impacting joint strength.[19] This study adopted a conservative plunge rate or speed of 2 mm/s, representing a relatively low speed. This decision was made to underscore the importance of thoroughly examining the impact of dwell time on the overall performance of the welded joint.

The FSW GG-7 model MTI equipment (Figure 1), located in the Light Structures Laboratory (LEL) of the Technological Research Institute (IPT) in the Technological Park of São José dos Campos – SP, was utilized for conducting the welds. This equipment was tailored for friction stir welding applications and features a large table with 3800 mm by 3900 mm and a robust capacity of 80 kN. It operates at tool rotational speeds up to 3000 r/min, advance speeds up to 3000 mm/min, and generates a torque of 280 Nm. A series of load cells are installed within the equipment to capture and record pertinent data regarding the forces exerted during the process.

The tools utilized in the process were made from a tungsten carbide class M30 material. The class M30 chemical composition was 10% Co, 0.5% TiC, and 89.5% WC, according to ISO 513.[20] The tool material presented a hardness higher than 950 HV_5 and a density of approximately 14.5 g/cm³, according to the tungsten carbide manufacturer Brassinter®. As illustrated in Figure 2, the pin geometry was designed to optimize shear stress resistance in the joints, considering the rigorous demands of automotive manufacturing. The pin was conically shaped.

The sheet samples for the process were cut using an abrasive waterjet to achieve dimensions of 105 mm in length and 45 mm in width, as depicted in Figure 3. This geometry was selected based on the shear test specifications outlined in the ISO14273:2016.[21] It allows for creating a 1.4 mm overlapping joint through the FSSW welding process.

Temperature measurements were captured using a T450 infrared thermal detector (FLIR) with an emissivity factor of 0.77.[22] The sensor spot was positioned on the front of the tool pin base, targeting the welding area, and the temperature values were acquired at a 10 Hz rate. The equipment used for metallographic analysis was a ZEISS Axio Scope A1 microscopy equipment, with a ZEISS Cr.3 camera and a TESCAN Scanning Electron Microscopy (SEM) equipment VEGA 3 LMU, with an energy detector dispersive spectroscopy. The tensile lap shear test was performed using a 250 kN servo-hydraulic MTS machine.

Results and discussion

The experimental results are presented in Table 2, while the corresponding analysis of variances (ANOVA) can

Figure 1. FSW, FSSW machine.
FSSW: friction stir spot welding; FSW: friction stir welding.

be found in Table 3. The performance of the joints showed a close correlation with the axial force and torque, which can be attributed to the energy input during the welding process. This energy input results from a combination of material plastic deformation and friction, increasing rapidly upon contact between the pin and the upper plate. The maximum energy input was observed when the tool's shoulder touched the upper plate's surface.[17]

The ANOVA revealed that the plunge depth was the only factor found to be statistically significant at a significance level of 5% (p-value < 0.05). Specifically, the highest axial force values were observed in runs 3, 4, 7, and 8, corresponding to a plunge depth of 1.07 mm, as indicated in Table 2. These force values ranged from 14 to 17 kN. These increased forces at maximum plunge depth can be attributed to the volume of material present in the mixing zone, where the tool's stirring action can determine heat flux by rotating the material[4] and the pressure exerted by the plastically deformed region.

Table 3 presents the ANOVA aiming to assess the statistical significance of multiple factors and their interactions in the responses of lap-shear force, axial force, torque, and temperature. The F-statistic and p-value values were used as metrics to determine the significant factors that impact the responses; the bold values indicate the significant condition to be addressed to the factors (1) tool rotational speed, (2) plunge depth, (3) dwell time or their combinations, (L) means a linear relationship, and (Q) means a quadratic relationship modelled by the response surface method.

Temperature: Significant influence was observed only for tool rotational speed (L) in predicting the temperature, with a considerable F-statistic and a low p-value. The other factors and interactions did not significantly affect the temperature; Torque: tool rotational speed (L), tool rotational speed (Q), plunge depth (L), plunge depth (Q), dwell time (L), the interaction 1L by 3L, and the interaction 2L by 3L had a significant influence on the prediction of torque. These factors showed high F-statistics and low p-values, indicating relevance. The factors dwell time (Q) and the interaction 1L by 2L did not demonstrate significance; Axial force: Plunge depth (L), plunge depth (Q), and the interaction 2L by 3L were highly significant in predicting the axial force, with high F-statistic values and low p-values. This suggests that these factors are important in determining the axial Force. On the other hand, the remaining factors and interactions did not significantly influence; Lap-shear force: The factors tool rotational speed (L), tool rotational speed (Q), plunge depth (L), plunge depth (Q), dwell time (L), dwell time (Q), and their interactions 1L by 2L, 1L by 3L, 2L by 3L, did not show significant influence.

The torque values were significantly influenced by both the plunge depth and tool rotational speed, as indicated in Table 3. In most tests, the torque remained relatively stable, ranging from 35 to 50 Nm. Test 8, which involved a tool rotational speed of 1900 r/min, a plunge

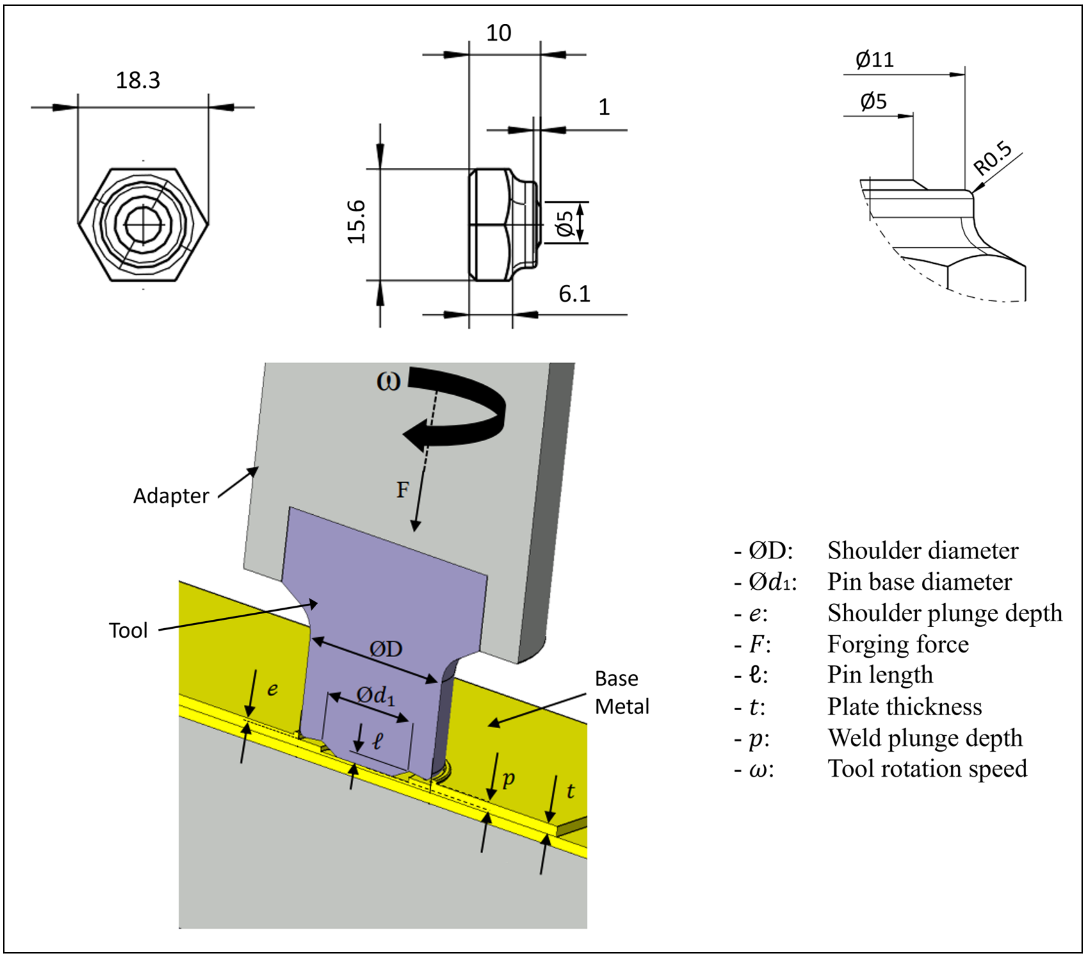

Figure 2. Schematic friction stir spot welding (FSSW) tool geometry.

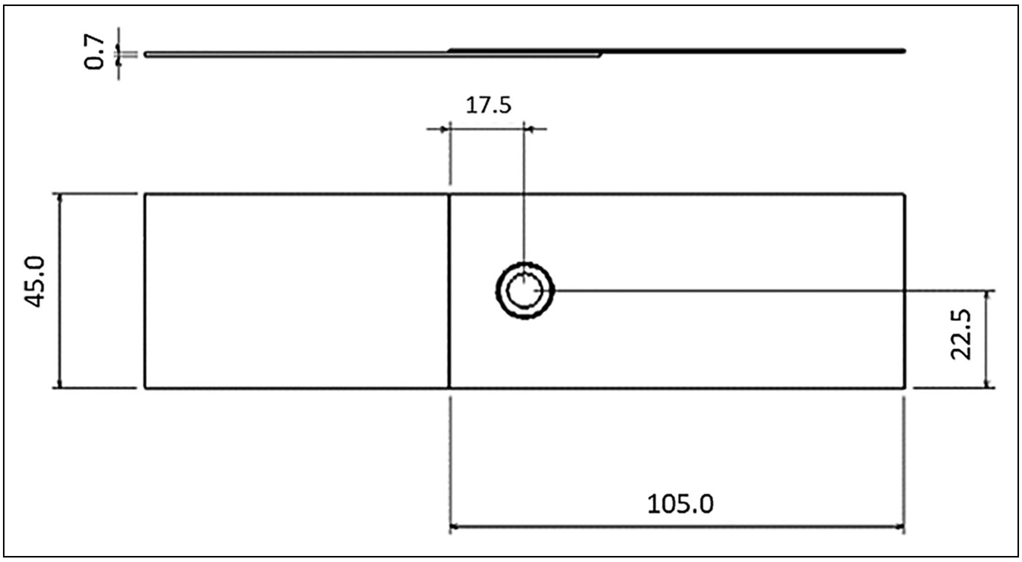

Figure 3. Dimensions of lap shear tensile specimens.

depth of 1.07 mm, and a dwell time of 5 s, exhibited the highest torque peak along with the critical axial force. Conversely, test 11 had the lowest torque value, featuring a tool rotational speed of 1700 r/min, a plunge depth of 0.80 mm, and a dwell time of 4 s. The torque, plunge depth, and tool rotational speed values are interconnected with the material flow within the mixing zone. A larger volume of material, resulting from a greater plunge depth, increases friction and consequently requires higher torque from the tooling to plastically

Table 2. Response surface methodology results.

Run	Tool rotational speed (r/min)	Plunge depth (mm)	Dwell time (s)	Temperature Max(°C)	Lap-shear force (N)	Axial force Max(N)	Torque (Nm)
1	1500	0.87	3.0	944.72	7212.79	11441.41	33.02
2	1500	0.87	5.0	536.86	7288.30	5990.24	33.50
3	1500	1.07	3.0	682.17	6380.21	13969.77	45.42
4	1500	1.07	5.0	476.68	8314.08	15396.27	47.80
5	1900	0.87	3.0	590.03	7669.78	10078.23	46.85
6	1900	0.87	5.0	497.21	7823.75	10284.76	50.24
7	1900	1.07	3.0	524.23	7594.27	16712.50	44.94
8	1900	1.07	5.0	497.64	6723.44	17063.47	67.94
9	1363	0.97	4.0	502.13	8325.85	13280.15	50.24
10	2036	0.97	4.0	726.69	8136.58	12966.90	47.80
11	1700	0.8	4.0	692.41	6661.66	9906.38	32.48
12	1700	1.14	4.0	790.99	7731.56	16507.08	50.24
13	1700	0.97	2.3	835.17	7960.06	14779.40	45.42
14	1700	0.97	5.7	808.36	6399.82	12954.96	46.37
15 C	1700	0.97	4.0	779.07	7439.32	13375.91	47.32
16 C	1700	0.97	4.0	934.76	8466.08	12223.34	46.37
17 C	1700	0.97	4.0	823.02	7755.1	11292.32	40.65
18 C	1700	0.97	4.0	927.42	6935.29	10816.57	45.89
19 C	1700	0.97	4.0	936.47	7418.61	9501.05	46.85

Table 3. Lap-shear force, axial force, torque, and temperature analysis of variance (ANOVA).

	Lap-shear force		Axial force		Torque		Temperature	
Factor	*F*-statistic	*p*-value	*F*-statistic	*p*-value	*F*-statistic	*p*-value	*F*-statistic	*p*-value
(1) Tool rotational speed(L)	0.021	0.892	1.597	0.275	**21.133**	**0.010**	0.099	0.759
Tool rotational speed(Q)	1.505	0.287	1.076	0.358	3.864	0.121	**12.190**	**0.006**
(2) Plunge depth(L)	0.159	0.710	**45.478**	**0.003**	**51.926**	**0.002**	0.194	0.669
Plunge depth(Q)	1.336	0.312	1.239	0.328	2.969	0.160	4.988	0.052
(3) Dwell time(L)	0.421	0.552	1.467	0.292	**9.364**	**0.038**	2.419	0.154
Dwell time(Q)	1.426	0.298	2.891	0.164	0.199	0.679	2.136	0.177
1L by 2L	0.735	0.440	0.128	0.739	2.015	0.229	0.455	0.516
1L by 3L	2.915	0.163	1.230	0.330	**9.374**	**0.038**	1.678	0.227
2L by 3L	0.273	0.629	2.889	0.164	**7.834**	**0.049**	0.496	0.498

Bold values indicate significant conditions related to the factors.

deform the mixing zone within the same time interval. Higher tool rotational speeds enable faster deformation rates, allowing for the assimilation of more material as the tool plunges plastically, as demonstrated by Lathabai et al.[19]

As shown in Table 2, at the highest tool rotational speed of 2036 r/min, the achieved temperature was 726 °C, while at the lowest tool rotational speed of 1363 r/min, a temperature of 502 °C was observed. Additionally, for the tool rotational speed of 1500 r/min runs, a temperature range of 477–945 °C was recorded, whereas the tool rotational speed of 1700 r/min exhibits temperature values ranging from 692 to 936 °C. The maximum temperature was observed for run #1, and the lower temperature was recorded for run #4.

Similar temperature patterns were observed by Andrade et al.[9] in their experimental and numerical study involving mild steel (DC01) under three galvanized conditions. In particular, the tool rotational speed of 1700 r/min played a critical role, resulting in maximum friction and a higher mixture flow, leading to elevated temperatures. This correlation can be observed in Table 2, specifically at the central points 16C–19C, indicating that the material reached complete phase transformation temperatures during the process. Notably, the temperature beneath the tool was higher due to the effects of friction and pressure. The temperature increase triggered a comprehensive recrystallization effect within the mixture zone, reducing work hardening and residual stresses.

The results obtained for the tensile lap-shear strength force did not exhibit statistical significance at a level of 5%. This indicates that the chosen tool profile and parameter range were robust in achieving an average tensile lap-shear force of 7.48 kN, as presented in Figure 4 by the blue dashed line. All the static tensile lap-shear test trials exhibited force values exceeding 6.0 kN. Runs #4, #9, #10, and #17 surpassed 8.0 kN. The average force

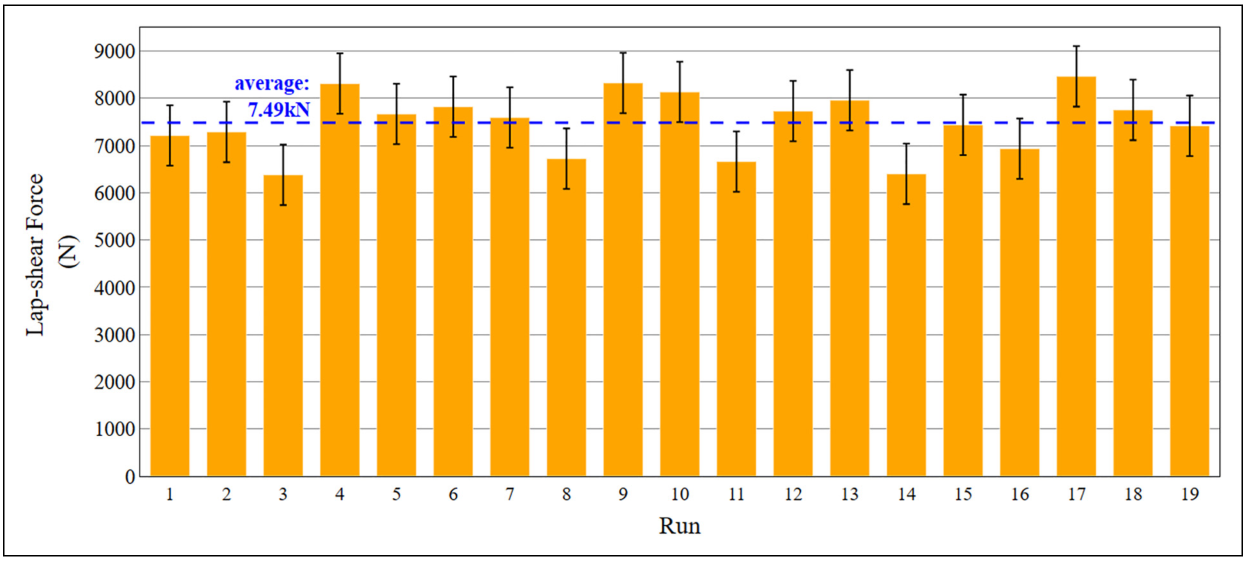

Figure 4. Lap-shear force for all runs, centring around the main average value of 7.49 kN.

Figure 5. Tensile lap-shear force test #2.

values obtained from the static tensile lap-shear test were 7.48 ± 0.64 kN. This reinforces that within the parameter range utilized for the FSSW process, it's viable to achieve highly resilient joints that exceed the minimum specification stipulated in the American National Standard AWS D8.1M:2021 of 1.5 kN (2).

These values are comparable to those reported by Baek et al.[15] of 3.4 kN. It is known that the tensile lap-shear force increases with the increase of tool rotational speed, plunge depth, and dwell time and then decreases.[13] This behaviour is influenced by variations in process parameters and the failure mode of the joints. The maximum

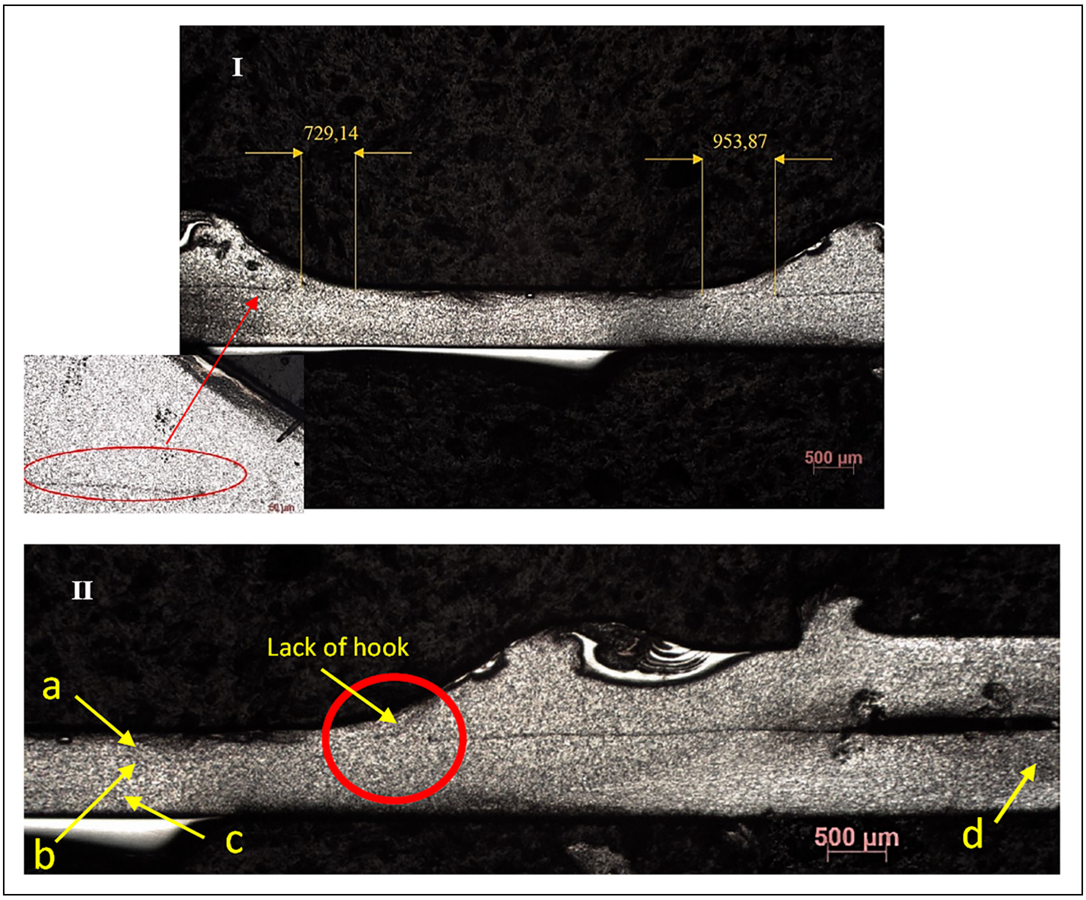

Figure 6. Run #19C: (I) width measurement; (II) lack of hook detail.

size of the mixing zone increases with rotation speed, resulting in a decrease in tensile shear force and a preference for shear fracture. However, higher tool rotational speeds leads to temperature rises,[5] and increased mixing zone size contributes to greater tensile shear force. Additionally, it is observed that high temperatures and long dwell times promote grain growth in the agitation region, which affects the mechanical properties of the joint. Ozdemir et al. successfully welded dissimilar metals using a friction stir spot welding process. They observed deformed grains close to the interface plates and recrystallization of the grains in the stir welding zone. Hardness was increased in the joint's bottom zone of the pin hole because of heat generation by the rotational pin tool. Additionally, when the depth of the plunge increases, the grain size decreases, leading to an increased hardness,.[23] Kumar et al.[8] observed high-strength joints where the bonding of grains between two materials was tightly compacted. The grains formed were almost the same size, and the stir zone displayed more smooth and acicular grains. On the other hand, low tensile strength has occurred due to large grain sizes that overlap and intend to form poor bonding,. Therefore, the synergy between the process variables influences the tensile shear force.

An important observation to note is that the failure mode observed in the tensile lap-shear force tests showed that all specimens experienced a ductile failure, even in test #2, where the plunge depth and tool rotational speed were at lower values, at 0.87 mm and 1500 r/min, respectively. In all tests, there was no complete rupture in the central region below the pin, as presented in Figure 5. This indicates that the resistance of the joint was distributed across the entire area beneath the tool's shoulder.

The values of tensile lap-shear force can be attributed to the flow characteristics within the mixing zone, which are influenced by the angle of the conical pin. The pin's geometry affects the shape of the hook, as illustrated in Figure 6. Notably, the absence of the hook can be observed, contributing to excellent resistance against tensile lap-shear forces. This favourable outcome is likely achieved through the angular mixing flow facilitated by the tool profile, which differs from the vertical flow observed with conventional tools, as described by Babu et al.[24]

The combination of tool rotational speed and plunge depth parameters, specifically around 1700 r/min and 0.97 mm, promoted significant temperature increases, overtaking the lower critical temperature value for steel, enabling phase change, recrystallizing, and other thermal structural transformation mechanisms,.[25,26] In Figure 6. I, the mixing zone for run 19C shows the absence of a hook at distances of 729 and 954 mm, indicating a complete connection between the plates due to material recrystallization (at a temperature of 936 °C), thereby increasing

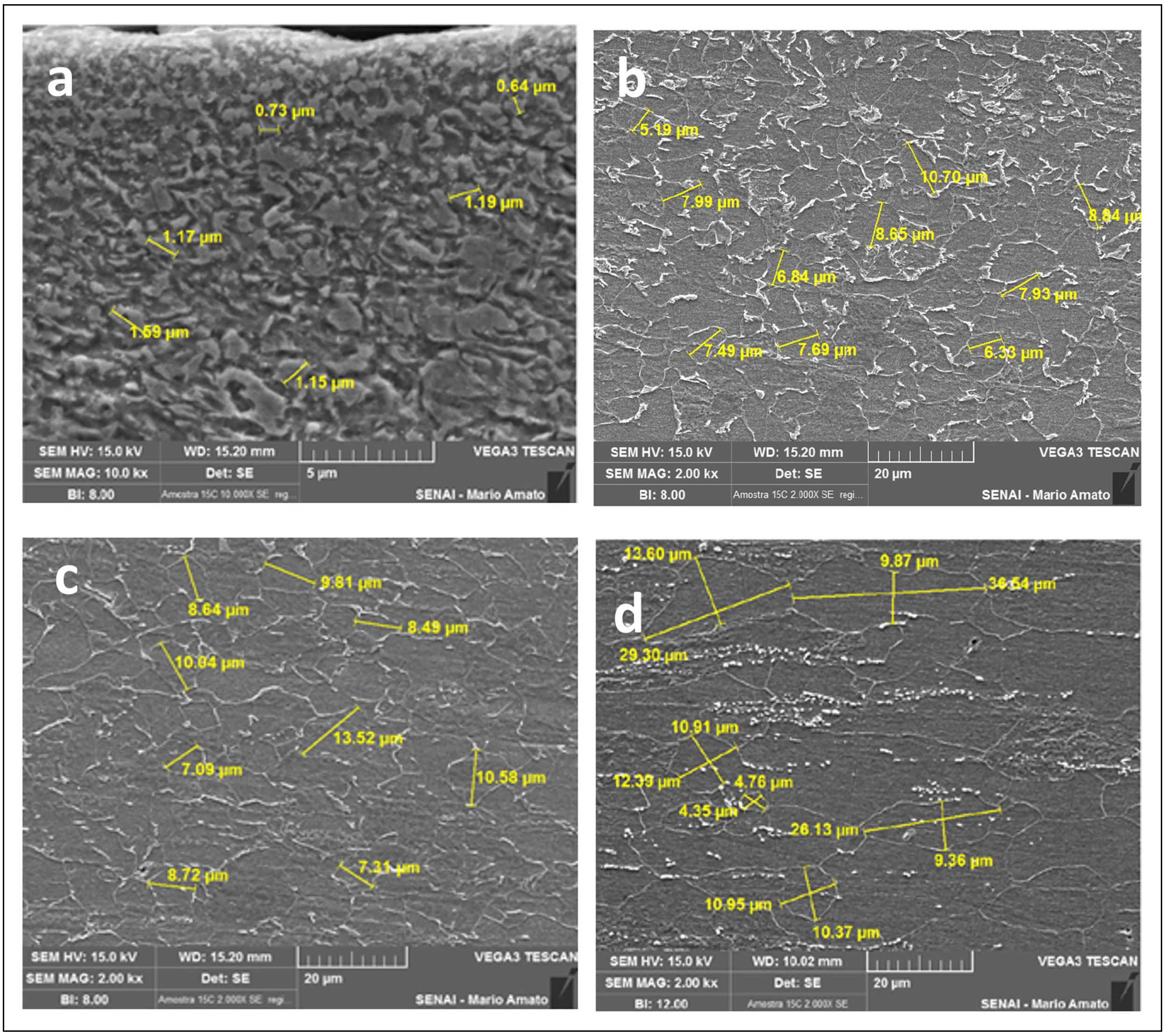

Figure 7. Run #19 C for microstructures and SEM evaluating: (a) MZ, (b) TMAZ, (c) TMAZSD, and (d) BM.
SEM: scanning electron microscopy; MZ: mixing zone; TMAZ: thermomechanical affected zone; TMAZSD: thermomechanical affected zone close to the sacrifice disc; BM: base material.

the joint's resistance and justifying the high tensile shear force values. Considering that the shear failure mechanism originates from the end of the intersection line between the two plates, known as the hook region, as mentioned by Babu et al.,[24] it can be observed in Figure 6. II that the interface line created by the mixing zone does not intersect with the keyhole. Therefore, it can be inferred that the shear-resistant interface approximately corresponds to the circumferential area below the pin.

Material recrystallization within the lack of a hook zone (MZ) (Figure 6. II) occurs below the pin in the weld's cross-section, resulting from the high cooling rate of the material and the presence of grains with a diameter smaller than 1.07 µm as can be observed in Figure 7(a).

In Figure 7(b), the thermomechanically affected zone (TMAZ) is observed, where the average grain size was approximately 8 µm, nearly eight times larger than the mixing zone (MZ). In the vicinity of the sacrifice disc, Figure 7(c), the TMAZ displayed an average grain size of 9 µm.

The microstructural analysis of the weld cross-section reveals distinct zones with varying grain sizes and characteristics. Within the lack of a hook zone (MZ), material recrystallization occurs beneath the pin due to the plastic work hardening effects of material friction and mixture followed by rapid material cooling leading to the presence of fine grains (Figure 7(a)). Moving outward from MZ, the TMAZ in Figure 7(b) exhibits an average grain size of about 8 µm, significantly larger than MZ, suggesting possible grain growth facilitated by high-temperature conditions due to heat flux by rotating the vicinity material and lower mixing pressure levels. Near the sacrifice disc (TMAZSD – Figure 7(c)), similar pressure conditions despite lower temperatures as MZ should observed, potentially influencing grain size. Both in TMAZ and TMAZSD, the plastic work hardening effects of material friction and mixture in the structure are not present. The BM region in Figure 7(d) displays an average grain size of around 17 µm, approximately an order of magnitude larger than that found in the MZ, displaying characteristic grains from the primary processing of sheet rolling process.

Conclusions

In this study, FSSW welding was conducted on lap joints using low-carbon steel, which is extensively employed in the automotive industry. This research aimed to assess the mechanical characteristics of the joints of the developed tool profile. The following conclusions were drawn:

- The combination of tool rotational speed and plunge depth parameters, specifically around 1700 r/min and 0.97 mm, promoted significant temperature increases, overtaking the lower critical temperature for steel value, enabling phase change, recrystallizing, and other thermal structural transformation mechanisms.
- The chosen range of variables provided a reasonable approach for producing FSSW joints in low-carbon steel. The results obtained for the tensile lap-shear strength force did not exhibit statistical significance. This indicates that the chosen tool profile and parameter range were robust in achieving an average tensile lap-shear force of 7.48 kN $\pm$ 0.64kN.
- The failure mode observed in the tensile lap-shear force tests showed ductile failure in all specimens, indicating that the resistance of the joint was distributed across the entire area beneath the tool's shoulder.
- The absence of a hook in the MZ contributes to excellent resistance against tensile lap-shear forces, and material recrystallization within this zone increases the joint's resistance and justifies the high tensile shear force values.

Author contributions

All authors contributed to the study's conception and design. Material preparation, data collection, and analysis were performed by Carlos Eduardo Ciardi Barbosa, Sergio Delijaicov, and Adalto Farias. The first draft of the manuscript was written by Sergio Delijaicov, and all authors commented on previous versions of the manuscript. All authors read and approved the final manuscript.

Declaration of conflicting interests

The authors declared no conflicts of interest with respect to the research, authorship, and/or publication of this article.

Funding

The authors received no financial support for the research, authorship, and/or publication of this article.

ORCID iDs

Éd C Bordinassi https://orcid.org/0000-0002-3915-3077
Sergio Delijaicov https://orcid.org/0000-0001-5621-9536

References

1. AWS D8.1 M. Specification for automotive weld quality - Resistance spot welding of steel. American Welding Society. 2021.
2. DIN EN 10139. Cold rolled uncoated mild steel narrow strip for cold forming. 1997.
3. Feizollahi V and Moghadam AH. Results in materials effect of pin geometry, rotational speed, and dwell time of tool in dissimilar joints of low-carbon galvanized steel and aluminum 6061-T6 by friction stir spot welding. *Results Mater* 2023; 20: 100483.
4. Bahedh AS, Mishra A, Al-Sabur R, et al. Machine learning algorithms for prediction of penetration depth and geometrical analysis of weld in friction stir spot welding process. *Metall Res Technol* 2022 Jun 8; 119: 05.
5. Al-Sabur RK and Jassim AK. Friction stir spot welding applied to weld dissimilar metals of AA1100 Al-alloy and C11000 copper. *IOP Conf Ser Mater Sci Eng* 2018; 455. DOI: 10.1088/1757-899X/455/1/012087.
6. Çapar N, Kumru U, Baser TA, et al. Friction stir spot welding for automotive applications. *Int J Adv Automot Technol* 2017; 1: 114–118.
7. Kyffin W, Threadgill P, Lalvani H, et al. Progress in FSSW of DP 800 high strength automotive steel. Proc 6th Int Symp Frict Stir WeldingAt Montr Canada. 2006;(January).
8. Kumar CL, Jayakumar V, Bharathiraja G, et al. Parameter optimization and microstructure evaluation of welding of structural steel 1020 and AA6062. *Mater Res Express* 2023; 10. DOI: 10.1088/2053-1591/acb120.
9. Andrade DG, Sabari SS, Leitão C, et al. Influence of the galvanized coating thickness and process parameters on heat generation and strength of steel spot welds. *Thin-Walled Struct* 2021; 160. DOI: 10.1016/j.tws.2020.107401.
10. Yang XW, Fu T and Li WY. Friction stir spot welding: a review on joint macro- and microstructure, property, and process modelling. *Adv Mater Sci Eng* 2014; 2014. DOI: 10.1155/2014/697170.
11. Wang X, Morisada Y and Fujii H. Flat friction stir spot welding of low carbon steel by double side adjustable tools. *J Mater Sci Technol* 2021; 66: 1–9.
12. Wang X, Morisada Y, Ushioda K, et al. Double-sided friction stir spot welding of ultra-high strength C-Mn-Si martensitic steel by adjustable probes. *J Mater Process Technol* 2022; 300: 117422.
13. Lakshminarayanan AK, Annamalai VE and Elangovan K. Identification of optimum friction stir spot welding process parameters controlling the properties of low carbon automotive steel joints. *J Mater Res Technol* 2015; 4: 262–272.
14. Sun YF, Fujii H, Sato Y, et al. Friction stir spot welding of SPCC low carbon steel plates at extremely low welding temperature. *J Mater Sci Technol* 2019; 35: 733–741.
15. Baek SW, Choi DH, Lee CY, et al. Structure-properties relations in friction stir spot welded low carbon steel sheets for light weight automobile body. *Mater Trans* 2010; 51: 399–403.
16. Feng Z, Santella ML, David SA, et al. Friction stir spot welding of advanced high-strength steels - a feasibility study. *SAE Transactions* 2005; 114: 592–598.
17. Mazzaferro CCP, Rosendo TS, Tier MAD, et al. Microstructural and mechanical observations of galvanized

TRIP steel after friction stir spot welding. *Mater Manuf Process* 2015 Sep 2; 30: 1090–1103.
18. Gerlich A, Avramovic-Cingara G and North TH. Stir zone microstructure and strain rate during Al 7075-T6 friction stir spot welding. *Metall Mater Trans A Phys Metall Mater Sci* 2006; 37: 2773–2786.
19. Lathabai S, Painter MJ, Cantin GMD, et al. Friction spot joining of an extruded Al-Mg-Si alloy. *Scr Mater* 2006; 55: 899–902.
20. ISO 513. Classification and application of hard cutting materials for metal removal with defined cutting edges. 2012.
21. ISO 14273. Resistance welding — Destructive testing of welds – Specimen dimensions and procedure for tensile shear testing resistance spot and embossed projection welds. 2016.
22. Bramson MA. *Infrared Radiation*. Boston, MA: Springer US, 2013.
23. Özdemir U, Sayer S and Yeni Ç. Effect of pin penetration depth on the mechanical properties of friction stir spot welded aluminum and copper. *Mater Test* 2012; 54: 233–239.
24. Babu S, Sankar VS, Janaki Ram GD, et al. Microstructures and mechanical properties of friction stir spot welded aluminum alloy AA2014. *J Mater Eng Perform* 2013; 22: 71–84.
25. Matjeke VJ, van der Merwe JW and Vithi NL. Determination of critical transformation temperatures for the optimisation of spring steel heat treatment processes. *Metals (Basel)* 2021; 11: 1–14.
26. Zhao W and Zhang Y. Prediction of transition temperature of alloy steel austenite based on self-organizing neural network. *IOP Conf Ser Mater Sci Eng* 2019; 563. DOI: 10.1088/1757-899X/563/2/022042.